Local circadian clock gates cell cycle progression of transient amplifying cells during regenerative hair cycling

Maksim V. Plikus[a,b], Christopher Vollmers[c], Damon de la Cruz[a], Amandine Chaix[c], Raul Ramos[b], Satchidananda Panda[c,1], and Cheng-Ming Chuong[a,1]

[a]Department of Pathology, Keck School of Medicine, University of Southern California, Los Angeles, CA 90033; [b]Department of Developmental and Cell Biology, Sue and Bill Gross Stem Cell Research Center, University of California, Irvine, CA 92697; and [c]Regulatory Biology Laboratory, Salk Institute for Biological Studies, La Jolla, CA 92037

Edited by Joseph S. Takahashi, Howard Hughes Medical Institute, University of Texas Southwestern Medical Center, Dallas, TX, and approved April 18, 2013 (received for review September 24, 2012)

Regenerative cycling of hair follicles offers an unique opportunity to explore the role of circadian clock in physiological tissue regeneration. We focused on the role of circadian clock in actively proliferating transient amplifying cells, as opposed to quiescent stem cells. We identified two key sites of peripheral circadian clock activity specific to regenerating anagen hair follicles, namely epithelial matrix and mesenchymal dermal papilla. We showed that peripheral circadian clock in epithelial matrix cells generates prominent daily mitotic rhythm. As a consequence of this mitotic rhythmicity, hairs grow faster in the morning than in the evening. Because cells are the most susceptible to DNA damage during mitosis, this cycle leads to a remarkable time-of-day–dependent sensitivity of growing hair follicles to genotoxic stress. Same doses of γ-radiation caused dramatic hair loss in wild-type mice when administered in the morning, during mitotic peak, compared with the evening, when hair loss is minimal. This diurnal radioprotective effect becomes lost in circadian mutants, consistent with asynchronous mitoses in their hair follicles. Clock coordinates cell cycle progression with genotoxic stress responses by synchronizing Cdc2/Cyclin B-mediated G_2/M checkpoint. Our results uncover diurnal mitotic gating as the essential protective mechanism in highly proliferative hair follicles and offer strategies for minimizing or maximizing cytotoxicity of radiation therapies.

proliferation | radiation therapy | hair cycle

Many biological events are rhythmic at different levels of organization, from cellular to behavioral. Diverse clock mechanisms have evolved to endow such rhythmic events with proper periodicity. The circadian clock helps organisms anticipate predictable daily changes in their environment and to prepare for diurnal and seasonal adaptations. Mechanistically, the circadian clock is based on the autoregulatory gene expression feedback loop in its core consisting of Clock/brain and muscle ARNT-like 1 (Bmal1)/neuronal PAS domain-containing protein 2 transcription factors that induce *Period* (*Per*)/*Cryptochrome* (*Cry*) genes expression, the protein products of which, in turn, inhibit these factors (1). Through its output mechanisms, the circadian clock generates daily fluctuations in various homeostatic processes (2). In mammals, a "master circadian clock" in the suprachiasmatic nucleus (SCN) uses both direct and indirect mechanisms to generate daily rhythms in several systemic signaling factors. In the peripheral tissues, local circadian clock also orchestrates intrinsic rhythms for their respective functions.

We wanted to examine the role of circadian rhythms in hair cycle, which is a complex regenerative process consisting of sequential phases of hair production (anagen), followed by hair follicle inactivity (telogen). The timing of anagen initiation and anagen cessation (also known as catagen) largely determine the length of this cycle. Following anagen initiation, proliferation of epithelial cells and terminal differentiation of their postmitotic progenies sustain continuous hair production. Catagen terminates hair growth and remodels hair follicle back into its inactive state of telogen. A complete hair cycle involves precise orchestration of cellular proliferation, migration, and differentiation in spatially defined populations of bulge stem cells, hair germ progenitors, transient amplifying cells of the matrix, and senescent cells of the hair shaft. The complexity of hair cycle offers several points of regulation by the circadian clock in different cell types and in different cellular processes (3, 4).

Several recent works started to uncover the role of circadian clock in hair follicle progenitor populations of bulge and hair germ (5–7). The pioneering study by Lin et al. (6) has identified hair germ as the key site of peripheral circadian activity in hair follicles during telogen and upon their transition into early anagen phase. Using *Clock* and *Bmal1* mutant mice, the authors revealed that circadian clock positively regulates activation of hair germ progenitors and that germ-line pathway mutations result in their temporary arrest in G_1 and cause delay of anagen initiation by up to several days. Intriguingly, a more recent study from the same research group showed that epithelial *Bmal1* deletion is insufficient to reproduce anagen initiation delay of the germ-line *Bmal1* knockouts, suggesting the presence of as-yet-unknown indirect circadian mechanism (8). In another study, Janich et al. (7) have shown that follicular bulge displays inherent circadian heterogeneity, featuring $Clock^{high}$ and $Clock^{low}$ subpopulations of stem cells. Normally, $Clock^{high}$ bulge stem cells are more prone to physiological activation than $Clock^{low}$ cells. In

Significance

Here, we show that cell autonomous circadian clock optimizes physiological regeneration of hair follicles by synchronizing mitotic progression in transient amplifying hair-matrix cells. The daily mitotic rhythm makes hairs grow faster in the morning than in the evening. Also, because of high sensitivity of mitotic cells to radiation, significantly greater hair loss occurs in the morning than in the evening following exposure to the same dose of γ-radiation. These results provide a roadmap for developing new radiation therapy protocols, when radiation cytotoxicity can be either minimized or maximized by timing its delivery throughout the course of the day.

Author contributions: M.V.P., C.V., A.C., S.P., and C.-M.C. designed research; M.V.P., C.V., D.d.l.C., A.C., and R.R. performed research; M.V.P., D.d.l.C., and S.P. contributed new reagents/analytic tools; M.V.P., C.V., D.d.l.C., R.R., S.P., and C.-M.C. analyzed data; and M.V.P., S.P., and C.-M.C. wrote the paper.

The authors declare no conflict of interest.

This article is a PNAS Direct Submission.

[1]To whom correspondence may be addressed. E-mail: panda@salk.edu or cmchuong@usc.edu.

This article contains supporting information online at www.pnas.org/lookup/suppl/doi:10.1073/pnas.1215935110/-/DCSupplemental.

constitutive *K14cre;Bmal1*$^{f/f}$ mutant mice, bulge stem cells become locked in a more dormant Clock^{low} state. The authors also showed that, mechanistically, this functional bulge heterogeneity is dependent on direct transcriptional targeting of at least wingless/int (WNT) and transforming growth factor β (TGFβ) signaling pathways by Bmal1.

Although the circadian clock is clearly implicated in modulating quiescence of bulge and hair germ progenitors, its role during active phase of hair regeneration (anagen) remains unknown. We were intrigued by several classic works that attempted to uncover time-of-day–dependent synchronicity in hair growth (9, 10). Therefore, we undertook this study to explore the role of circadian rhythms in actively growing hair follicles. Among various anagen hair follicle cell populations, we found that transient amplifying cells of epithelial matrix and dermal papillae fibroblasts display strongest circadian rhythmicity. By using inducible epithelium-specific *Bmal1* deletion mouse model, we identified that cell-autonomous clock in hair matrix generates daily mitotic rhythms. These mitotic rhythms, which appear to depend on circadian synchronization of G_2/M checkpoint, confer growing hairs with variable resistance to genotoxicity throughout the day. We showed that by simply timing γ-radiation to the time of the day with lowest mitotic activity, a dramatic radioprotective effect can be achieved in wild-type (WT) mice, and radiation-induced hair loss can be largely prevented across the spectrum of γ-radiation doses. This radioprotective effect becomes lost in circadian mutants, which show significant hair loss in response to the same dose γ-radiation at different times of the day. We also established that although gating daily mitotic progression, clock has no effect on the total mitotic output of growing hair follicles. Hairs of circadian mutants are remarkably similar in length to WT hairs, and, thus, additional noncircadian mechanism operating in hair follicle precortex likely prevents mitotic surplus. This work reveals how circadian clock confers genotoxic protection during physiological regeneration of hair follicles by synchronizing daily cell cycle progression in rapidly proliferating epithelial matrix cells.

Results

Peripheral Circadian Rhythms Are Highly Compartmentalized in Anagen Hair Follicles. We used a combination of expression profiling and genetic approaches to define microanatomical distribution of peripheral circadian oscillators in regenerating hair follicles. We started by analyzing luciferase activity from cultured specimens of *Per2*^{Luc} skin and individual microdissected vibrissae follicles. In *Per2*^{Luc} mouse, Per2–Luciferase translational fusion protein is expressed from the native *Per2* promoter, such that longitudinal measurements of bioluminescence truly reflect the robustness and periodicity of the circadian oscillator (11). In agreement with the previous report by Lin et al. (6), skin with telogen hair follicles displayed clear circadian rhythms (Fig. 1*A*). Strong circadian oscillations were also produced for up to 4 d in culture by *Per2*^{Luc} anagen skin (Fig. 1*B*) and by microdissected anagen vibrissae follicles (Fig. 1*C*). Oscillation amplitude from all cultured samples dampened over time, likely because of desynchronization of the oscillators in individual cells and/or progressive cell death in vitro.

Time-lapse luminescence image analysis of individual cultured *Per2*^{Luc} vibrissae (Fig. 1 *D* and *E* and Movies S1, S2, S3, and S4) identified bulge (Fig. 1*F*) and bulb (Fig. 1*G*) as the most notable sites of active circadian rhythms in anagen hair follicles. Whereas the presence of clock in bulge was in agreement with previous report Janich et al. (7), bulb emerged as another high-circadian activity spot specific to regenerating anagen hair follicles. Next, we profiled expressions of Per2, Clock, and Npas2 proteins to further define microanatomical distribution of circadian oscillators. Using immunostaining approach, we focused on differentiating between nuclear, cytoplasmic, and mixed nuclear/cytoplasmic expression patterns versus lack of expression (Figs. S1–S3). This approach was chosen over expression measurements on sorted cell populations, because current cell sorting protocols are unable to differentiate between many key anagen hair follicle subcompartment. Because Per2 levels peak around subjective dusk in most peripheral tissues (2, 11), we collected vibrissae and pelage skin samples from WT C57BL/6J mice at different circadian time points (CTs) centered at CT58. Overall Per2 expression along the anagen vibrissae paralleled the Per2^{Luc} signal from our in vitro experiments; higher levels of Per2 expression were found in the bulge and bulb with little expression in between (Fig. S1). Notably, within vibrissae and pelage hair follicle bulbs circadian proteins were prominently expressed both by transient amplifying cells of epithelial matrix and by fibroblasts of dermal papillae. Matrix cells displayed very strong Per2 expression which was distinctly rhythmic (Fig. 2 *A* and *E*). Clock expression in the matrix was also strong, rhythmic, and antiphasic with Per2 (Fig. S3*G*). Similarly, both Per2 and Clock displayed strong, rhythmic, and mutually antiphasic expressions in dermal papillae fibroblasts (Fig. 2 *A* and *E* and Fig. S3*H*). Npas2 was selectively absent from both matrix and dermal papilla (Fig. S3 *O* and *P*). For a detailed guide into Per2, Clock, and Npas2 expression patterns in other hair follicle compartments, see Figs. S2 and S3.

Cell-autonomous Circadian Clock Generates Daily Mitotic Rhythm in Matrix of Anagen Hair Follicles. We were intrigued by the early study by Comaish (9) and some anecdotal evidence suggesting that the speed of human hair growth is uneven throughout the day and that, in fact, hairs grow faster during the day than at night. Because we have identified that peripheral clock is robust both in epithelial matrix and in dermal papilla, we hypothesized that circadian oscillator in one of these compartments generates daily proliferation rhythm that results in diurnal hair-growth speed changes.

Transient amplifying matrix cells are highly proliferative, and in agreement with the recent study by Geyfman et al. (8), we were unable to detect clear differences in the numbers of proliferating cell nuclear antigen (Pcna)-positive cells in WT pelage hair-follicle matrixes between different CTs. To determine whether daily variations in matrix proliferation occur specifically at the level of mitoses, we performed histomorphometric analysis of phospho-histone H3 (pH3)-positive cells in WT anagen hair follicles. Our data revealed clear circadian rhythm of mitotic cells in the matrix (Fig. 3 *A*–*D*). Numbers of pH3-positive mitotic cells in pelage anagen hair follicles were the highest at subjective morning (CT50 and CT70) and declined by 50–70% at subjective evening (CT58, CT62) (Fig. 3*D*, blue bars). Similar dynamics were also observed in anagen vibrissae follicles (Fig. 3*C*).

Next, we wanted to establish whether these daily mitotic differences disappear in circadian mutants. We started by examining circadian oscillator-deficient *Cry1*$^{-/-}$;*Cry2*$^{-/-}$ mice. At first we showed that the loss of Cry proteins in these mutants leads to cessation of circadian rhythmicity and results in constitutively high levels of Per2 and Clock proteins in all compartments of both pelage and vibrissae follicles (Fig. 2 *B* and *F* and Fig. S4). Additionally, none of the hair follicle compartments that are normally negative for Per2 showed Per2 expression in Cry deficient mice, thus implying the Cry proteins do not participate in the spatial determination of Per2 expression. Importantly, daily mitotic differences disappeared in *Cry1*$^{-/-}$;*Cry2*$^{-/-}$ hair follicles, where numbers of pH3-positive matrix cells at subjective morning (CT50) were comparable to those in WT, but failed to decline significantly at subjective evening (CT62) (Fig. 3 *C* and *D*, orange bars).

Next, we wanted to determine whether the daily mitotic output rhythm is an intrinsic property of matrix keratinocytes or

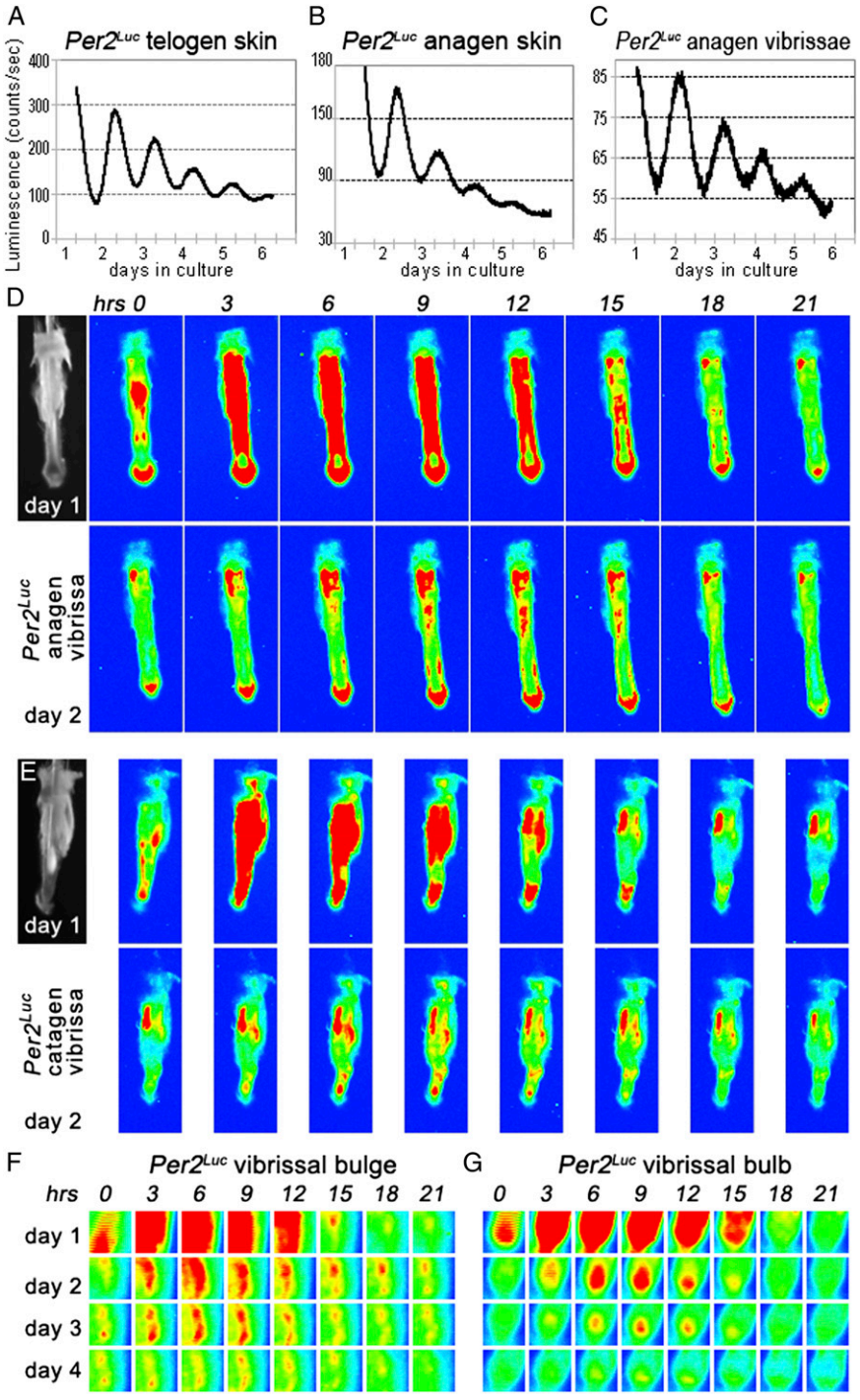

Fig. 1. $Per2^{Luc}$ reveals peripheral circadian rhythms in skin and anagen hair follicles. (*A* and *C*) In cultured $Per2^{Luc}$ mouse skin with either telogen (*A*) or anagen (*B*) hair follicles, luminescence levels change with circadian periodicity for at least 3–4 d. (*C*) This circadian periodicity is also displayed by cultured $Per2^{Luc}$ vibrissae. (*D–G*) Time-lapse photography of individually cultured $Per2^{Luc}$ vibrissae shows that circadian cycles of luminescence localize to several follicular areas, most prominently to follicular bulge (*F*) and bulb (*G*). To aid visualization, originally black-and-white images of luminescence levels were converted into heat maps, so that areas of highest luminescence appear red, and areas with no luminescence appear blue, with blue–green–yellow–red gradient in between. Sequential snapshots shown here are 3 h apart. Microdissected vibrissae at time point zero are shown for *D* and *E*. Also see Fig. S1.

whether, instead, it is driven by the dermal papillae and/or SCN circadian clock. Systemic disruption of circadian oscillators in Cry-deficient mice does not allow differentiation between local versus systemic clock inputs. To overcome this limitation, we generated a *K14creER;Bmal1*$^{f/f}$ mouse, where tamoxifen-inducible deletion of *Bmal1* in epithelial but not mesenchymal follicular compartments during telogen allows studying anagen hair follicles during the next hair cycle with "oscillator^{-}" matrix and "oscillator^{+}" dermal papilla (Fig. 2*C*). At first we examined the effect of induced epithelial *Bmal1* deletion in both vibrissa and pelage follicles (induction efficiency was verified in *K14creER;R26R* mice as detailed in *Methods*). Indeed, *Bmal1* deletion largely abolished circadian expressions of both Per2 and Clock throughout skin epithelia. Per2 became undetectable in epidermis and yet remained high and arrhythmic between CT50 and CT62 in hair-follicle matrix. In contrast, dermal papillae maintained normal cyclic Per2 expression, which peaked at CT62 (Fig. 2 *D* and *G* and Fig. S5). Cyclic Clock expression was also lost in all epithelial structures of *K14creER;Bmal1*$^{f/f}$ vibrissae but not in the dermal papilla, where it peaked at CT50 (Fig. S5). We observed similar loss of daily mitotic output rhythm in hair follicles of induced *K14creER;Bmal1*$^{f/f}$ mice as we saw in *Cry1*$^{-/-}$;*Cry2*$^{-/-}$ mutants (Fig. 3 *C* and *D*, green bars),

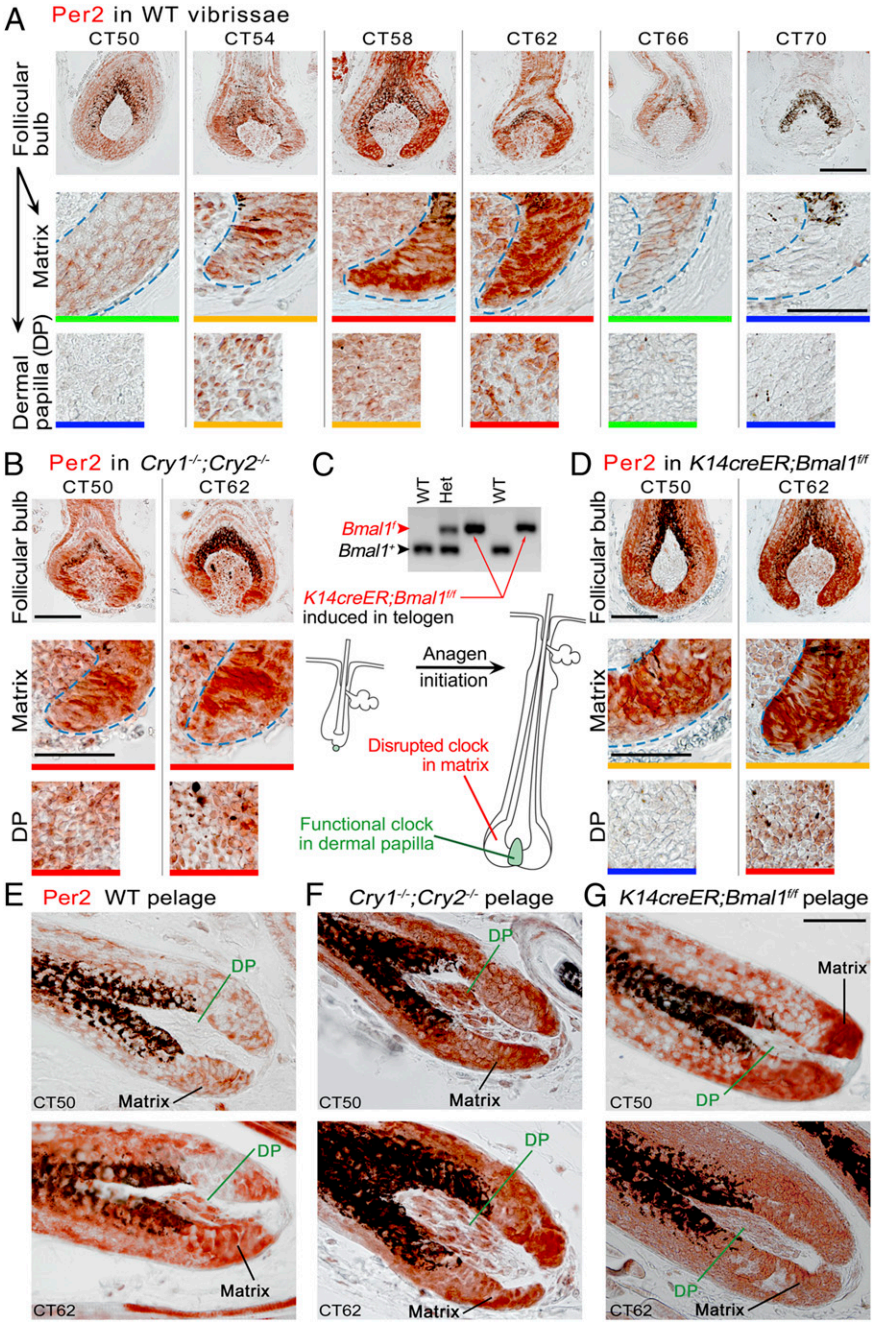

Fig. 2. Epithelial matrix and dermal papilla constitute key sites of circadian activity in anagen hair follicles. (*A* and *E*) Very prominent circadian expression cycles of Per2 exist in the bulb of WT anagen hair follicles. Per2 peaks at CT58 and CT62 and is at its lowest, or absent, at CT50 and CT70 in epithelial matrix and mesenchymal dermal papilla. (*B* and *F*) In matrix and dermal papilla of *Cry1*$^{-/-}$;*Cry2*$^{-/-}$ hair follicles, Per2 expression becomes high and arrhythmic. (*C*) Upon tamoxifen-inducible deletion of *Bmal1* in *K14creER;Bmal1*$^{f/f}$ mice, a functional circadian clock becomes lost in epithelial but not mesenchymal skin cell types. During anagen, the circadian clock is not functional in epithelial matrix cells and their differentiated progenies. It remains functional in dermal papilla. (*D* and *G*) In induced *K14creER;Bmal1*$^{f/f}$ hair follicles, Per2 expression becomes high and arrhythmic in epithelial matrix at CT50 and CT62. Dermal papillae maintain normal cyclic Per2 expression, which peaks at CT62. [Scale bars: 100 μm (*A*, *Top*); 50 μm (*A*, *Middle* and *Bottom*, *B*, and *D*–*G*).] Color bars at the bottom of each image define expression levels: blue, no expression; green, weak, mostly cytoplasmic expression; yellow, strong cytoplasmic and/or weak nuclear expression; red, strong nuclear or mixed nuclear/cytoplasmic expression. Also see Figs. S2–S5.

supporting that diurnal mitotic progression is an intrinsic feature of matrix keratinocytes.

To find out whether daily mitotic rhythm in hair matrix translates into daily variations in hair growth, we designed a 36-h 5-ethynyl-2′-deoxyuridine (EdU) pulse-chase experiment, where a single dose of EdU was administered to WT mice either at CT54 or CT66, which translates into 1300 and 0100 hours on the AM/PM timeline, respectively (Fig. S6). Pulse chasing for 36 h resulted in anagen hair follicles that grew either for two 12-h-long mitotic depressions and one 12-h-long mitotic peak (CT54 group) or for two mitotic peaks and one mitotic depression (CT66 group). We hypothesized that EdU incorporation will be found further along the growing hair shafts in hair follicles from CT66 group, reflecting higher cumulative mitotic activity during the additional mitotic peak period. Indeed, our analysis showed that EdU was incorporated into growing hair shafts on average 100 μm (or ∼four to five cell rows) higher in hair follicles from CT66 versus CT54 group ($n = 50$; $P < 0.001$), confirming the presence of diurnal hair-growth rhythmicity (Fig. 3 *E* and *F*).

Clock Gates Postmitotic Exiting but Not Total Mitotic Output of Matrix Keratinocytes. We then wondered whether mitotic asynchrony in hair matrixes of circadian mutants is associated with other proliferation defects. We examined broad spectrum of proliferating matrix cells based on Pcna expression. Normally, Pcna-positive cells are restricted to the proximal (lower) portion of hair matrix roughly demarcated by the Auber line. Position of the Auber line can be easily established as it coincides with the initiation of visible pigmentation (Fig. S7 *A*–*D*). The vast majority of Pcna-positive matrix cells in WT anagen hair follicles both at CT50 and CT62 were indeed located below the Auber

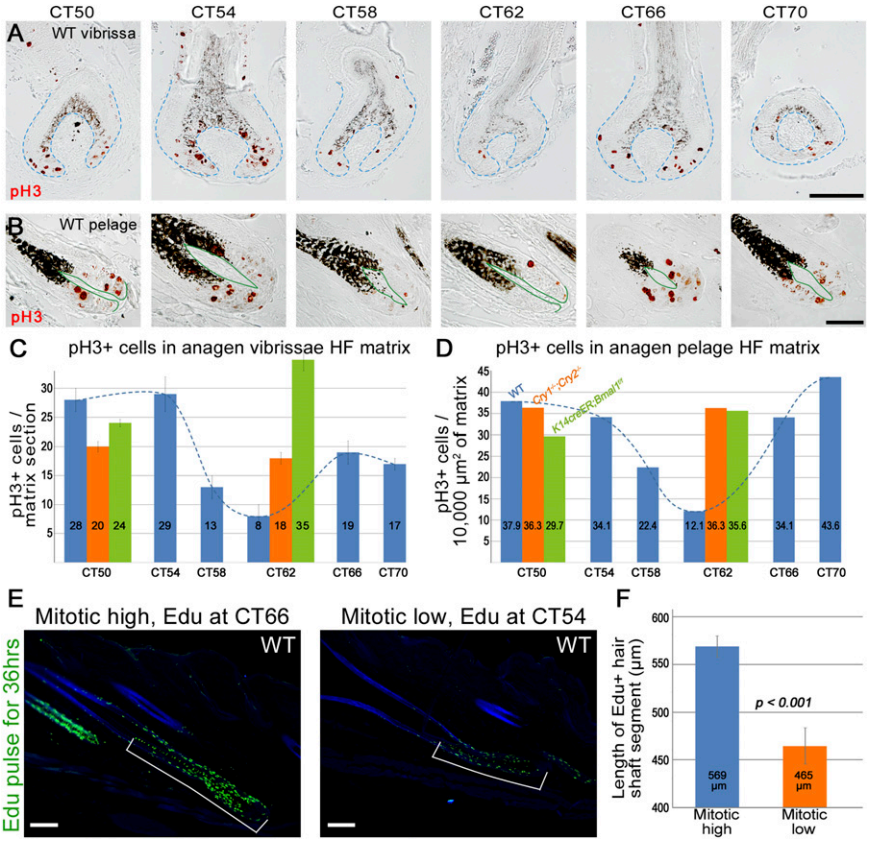

Fig. 3. Mitotic progression in hair-follicle matrix shows circadian rhythmicity. (*A* and *B*) Expression patterns of M phase-specific pH3 in WT anagen vibrissae (*A*) and pelage (*B*) hair follicles at different CTs. (*C* and *D*) Quantification of pH3-positive cells in matrixes of vibrissae (*C*) and pelage (*D*) hair follicles at different CT points. Average values are shown within the chart bars. Blue bars represent data from WT, orange bars represent *Cry1*$^{-/-}$*;Cry2*$^{-/-}$, and green bars represent induced *K14creER;Bmal1*$^{f/f}$ mice. (*E* and *F*) After pulse chasing for 36 h, WT anagen hair follicles incorporated EdU, on average, 100 μm higher along the hair shaft when EdU was administered at CT66 versus CT54. In the CT66 group, hair follicles grew for two 12-h-long mitotic peaks and one 12-h-long mitotic depression, whereas in the CT54 group, they grew for one mitotic peak and two mitotic depressions. [Scale bars: 100 μm (*A* and *E*); 50 μm (*B*).] Also see Fig. S6.

line, with only few Pcna-positive cells found immediately above it. In stark contrast, both *Cry1*$^{-/-}$*;Cry2*$^{-/-}$ and induced *K14creER;Bmal1*$^{f/f}$ anagen hair follicles showed significant expansion of Pcna-positive cells far above the boundaries of normal matrix (Fig. 4*A*). Ectopic Pcna-positive cells maintained high Per2 expression (Fig. 4*B*) and were preferentially distributed within the centermost layers of hair precortex and outermost layers of inner root sheath.

Next, we considered a possibility that this proliferation defect in circadian mutants results in a surplus of hair precortex cells. Consistent with this would be an overall increase in length and/or width of hair shaft and/or thickening of inner root sheath (12, 13). Additionally, onset of hair differentiation programs within precortex could be delayed and shifted upwards. To test this possibility, we performed careful measurements on telogen hair shafts (also known as club hairs) in WT and *Cry1*$^{-/-}$*;Cry2*$^{-/-}$ mice. Considering that the duration of anagen phase is not significantly changed in circadian mutants (6), length and width of club hairs can serve as reliable readout of total proliferative output of the follicular matrix. Our data show that the length of guard club hairs remains virtually identical between WT and *Cry1*$^{-/-}$*;Cry2*$^{-/-}$ mice: 10.2 ± 0.7 mm (n = 100) in WT and 10.4 ± 0.6 mm (n = 100) in *Cry1*$^{-/-}$*;Cry2*$^{-/-}$. Similarly identical are zigzag club hairs: 6.0 ± 0.4 mm (n = 100) in WT and 6.2 ± 0.2 mm (n = 100) in *Cry1*$^{-/-}$*;Cry2*$^{-/-}$ (Fig. 4 *C* and *D*). Vibrissae club hairs belonging to positionally identical follicles (Fig. S8; positions E, F, G, H, and AI through AV on the map of the mystacial pad were studied) slightly vary from hair to hair within the range of 0.4–2.8 mm (2–13%), with no significant length increases in *Cry1*$^{-/-}$*;Cry2*$^{-/-}$ mice (n = 53). There were also no significant hair shaft width changes, and we detected no significant expansion of inner root sheath in *Cry1*$^{-/-}$*;Cry2*$^{-/-}$ compared with WT anagen hair follicles. We then examined expression patterns of lymphoid enhancer-binding factor 1 (Lef1), which marks the onset of WNT-mediated differentiation program (Fig. S9*A*). We found no significant vertical shift in nuclear Lef1 expression domain among WT, *Cry1*$^{-/-}$*;Cry2*$^{-/-}$, and *K14creER;Bmal1*$^{f/f}$ hair follicles. Similarly, there was no vertical shift in AE15-positive hair shaft medulla and inner root sheath populations (Fig. S9*B*).

Consistent with the lack of hair length changes despite prominent vertical expansion of Pcna-positive matrix compartment is the possibility that precortex precursors are unable to complete ectopic mitotic divisions. Indeed, we have not observed ectopic pH3-positive precortex cells in our analysis of *Cry1*$^{-/-}$*;Cry2*$^{-/-}$ and *K14creER;Bmal1*$^{f/f}$ hair follicles. Similar to WT, pH3-positive mitotic cells in circadian mutants were restricted to proximal matrix below the Auber line. Prodifferentiation signaling via at least bone morphogenetic protein (BMP) and WNT pathways likely constitute a portion of this noncircadian mechanism. We show that many ectopic Pcna-positive precortex cells in *Cry1*$^{-/-}$*;Cry2*$^{-/-}$ hair follicles are simultaneously positive for phospho-Smad (pSmad)1/5/8 (Fig. 4 *E* and *F*) and Lef1 (Fig. 4 *G* and *H*).

Mitotic Rhythm Causes Dramatic Time-of-Day–Dependent Sensitivity of Growing Hairs to Irradiation. To understand physiological significance of circadian mitotic gating, we have considered the fact that proliferating cells are the most sensitive to various genotoxic stresses, especially to double-stranded DNA breaks, during M phase. Sensitivity to DNA damage during cell cycle declines in the following order: M → G_2 → G_1 → early S → late S (14–16) (Fig. 5*A*). Therefore, synchronization of mitotic progression in hair matrix outside the period of the day with higher genotoxicity would prove to be a beneficial adaptation. Solar irradiation is a well-established source of external genotoxicity in skin epidermis (8, 17); however, its impact on growing hair follicles is likely minimal considering that mice are largely nocturnal and have thick hair coats and because UV light does not penetrate skin to the depth of the hair matrix. Metabolic oxidative stress

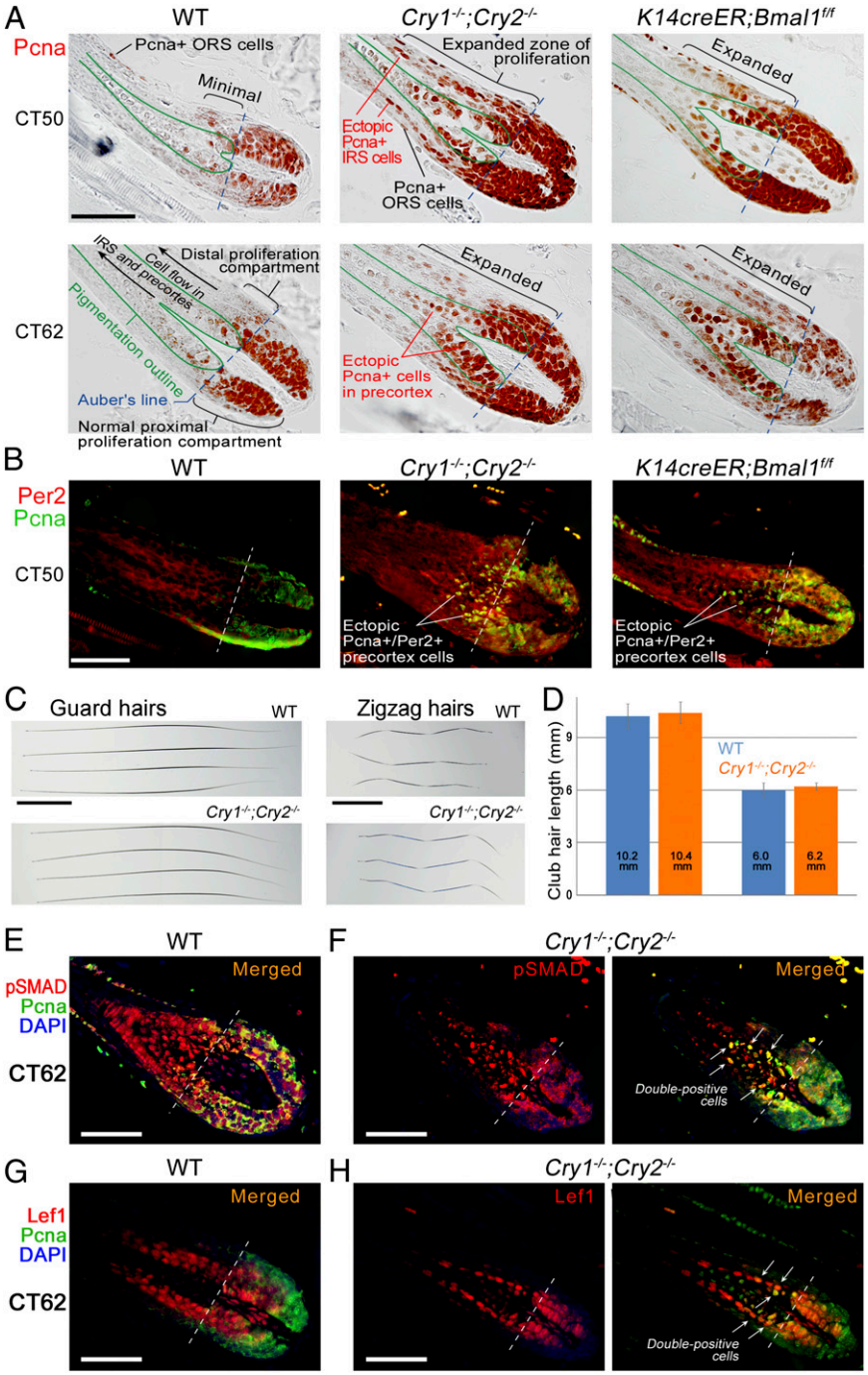

Fig. 4. Daily but not total mitotic output of hair-follicle matrixes is under circadian regulation. (*A* and *B*) Proliferative Pcna-positive cell population is expanded distally above the Auber line in *Cry1*$^{-/-}$;*Cry2*$^{-/-}$ and induced *K14creER;Bmal1*$^{f/f}$ anagen hair follicles compared with WT. Ectopic Pcna-positive cells in circadian mutants maintain strong Per2 expression (*B*). (*C* and *D*) Total length of dorsal guard and zigzag club hairs in adult *Cry1*$^{-/-}$;*Cry2*$^{-/-}$ mice does not differ significantly from these in WT mice. (*E* and *F*) A large proportion of ectopic Pcna-positive cells in precortex of *Cry1*$^{-/-}$;*Cry2*$^{-/-}$ hair follicles coexpresses markers of differentiation: pSmadD1/5/8 (*E* vs. *F*) and Lef1 (*G* vs. *H*). [Scale bars: 50 μm (*A*, *B*, and *E*–*H*); 2 mm (*C* and *D*).] Also see Figs. S8 and S9.

generates endogenous genotoxicity and its levels are known to undergo circadian fluctuations (8, 18, 19). Indeed, we show that hair-follicle matrix cells are subjected to oxidative damage, as shown by positive immunostaining of their nuclei for 8-hydroxy-2′-deoxyguanosine (8OHdG), a marker of oxidized DNA nucleosides (Fig. S9*C*).

Next, we designed an experiment in which WT mice with actively growing hair follicles were given various doses γ-irradiation, so that irradiation timing coincided with either mitotic peak (CT50) or mitotic depression (CT58). One week after irradiation, mice treated with 400–550 rad displayed significant differences in hair coat phenotypes between CT50 and CT58 groups (n = 10 in each group) (Fig. 5). Especially dramatic were differences after 500-rad irradiation dose. Although mice in the CT50 group were almost completely bald, mice in the CT58 group maintained most of their hair (Fig. 5*D*). Microscopically, 85 ± 1.9% of hairs were broken in mice from the CT50 group, whereas in the CT58 group, this number was only 17.4 ± 1% (Fig. 5*E*, red arrowheads). The rest of the hairs in mice from the CT58 group underwent various degrees of thinning (Fig. 5*E*, green arrowheads), yet remained intact. Majority of remaining unbroken hairs in mice from the CT50 group belonged to thicker guard hair type. Radiation-induced hair loss differences were maintained between CT50 and CT58 groups after up to 550 rad, but at higher doses of 600+ rad, mice in both groups displayed nearly complete depilation. This is likely because at 600+ rad doses, cytotoxic effect of γ-irradiation spreads across other cell cycle phases.

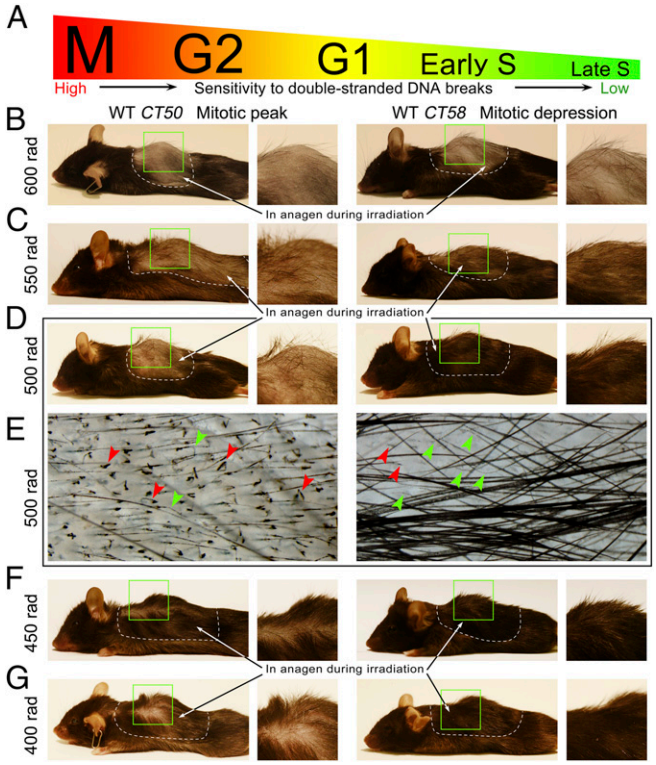

Fig. 5. Time-of-day–dependent sensitivity of growing hairs to irradiation. (*A*) Sensitivity of proliferating cells to double-stranded DNA breaks declines in the following order: M → G_2 → G_1 → early S → late S. (*B* and *G*) Hair follicles sustain different extent of radiation-induced damage depending on the time of the day. The same doses of γ-irradiation were administered to WT mice either at CT50 to coincide with mitotic peak or at CT58 to coincide with mitotic depression. Dramatic differences in terms of hair loss were observed for the 500-rad dose (*D* and *E*). Whereas in the CT50 group, 85% of hairs broke (red arrowheads on *E*), in the CT58 group, almost 83% of hairs were still intact, while undergoing various degrees of thinning (green arrowheads on *E*). Radiation-induced hair-loss differences between the CT50 and CT58 groups were also observed at 400-rad (*G*), 450-rad (*F*), and even 550-rad doses (*C*). A higher dose of radiation, 600 rad (*B*), caused nearly complete depilation in both the CT50 and CT58 groups.

We then wanted to verify that time-of-day–dependent sensitivity of growing hairs to ionizing radiation is indeed a function of circadian clock. We irradiated $Cry1^{-/-};Cry2^{-/-}$ mutant mice and $Cry1^{+/-};Cry2^{+/-}$ heterozygous control animals at CT50 and CT58 using a 500-rad dose. Remarkably, $Cry1^{-/-};Cry2^{-/-}$ mutants experienced severe hair loss at both time points with 90.8 ± 4% broken hairs at CT50 (n = 4) and 92.3 ± 1.4% at CT58 (n = 4) (Fig. 6*B*). This is in contrast to heterozygous control mice that maintained circadian radioprotective effect with 96.9 ± 1% hairs breaking at CT50 (n = 4) and only 22.9 ± 4.4% at CT58 (n = 4) (Fig. 6*A*). These results further verify physiological significance of circadian cell cycle synchronization in growing hair follicles.

Daily Mitotic Progression in Hair Matrix Is Synchronized at the G_2/M Checkpoint. To understand how circadian clock mechanism synchronizes cell cycle progression in the hair-follicle matrix, we have considered the following checkpoint mechanisms: cMyc and CyclinD1-mediated G_1/S checkpoint, and Wee1 and Cdc2/CyclinB-mediated G_2/M checkpoint and DNA damage-response checkpoint (20). Previously, cMyc expression was reported in matrix keratinocytes. We confirmed strong cMyc expression in the matrix and showed that it does not have circadian dynamics (Fig. S10*A*). Similarly, pCyclinD1 displayed constant expression patterns in both WT and $Cry1^{-/-};Cry2^{-/-}$ matrixes (Fig. S10*B*), thus making cMyc-mediated G_1/S checkpoint an unlikely mechanism of circadian synchronization of matrix proliferation.

G_2/M checkpoint can undergo circadian regulation via inhibitory phosphorylation of Cdc2 kinase on Tyr15 (pCdc2). Indeed, we observed nuclear pCdc2 expression patterns to have circadian characteristics in WT hair follicles: high at CT50 and low at CT62. Additionally, these circadian differences disappeared in matrixes of $Cry1^{-/-};Cry2^{-/-}$ hair follicles, where pCdc2 remains constantly high (Fig. 7*A*).

Next, we examined expression of γhistone H2A.X (H2AX), a sensitive marker of DNA double-strand breaks. We show that it also follows circadian dynamics. At CT50, the majority of WT matrix cells were γH2AX-negative, few cells showed "nuclear foci" expression patterns (Fig. 7*C*, green arrows), and only isolated cells had "pan-nuclear" expression (Fig. 7*C*, blue arrow). In contrast, at CT62, a large proportion of matrix cells was γH2AX-positive, showing "nuclear foci," various intensity "pan-nuclear," and mixed expression patterns. These circadian differences were abolished in $Cry1^{-/-};Cry2^{-/-}$ and *K14creER;* $Bmal1^{f/f}$ hair follicles that maintained γH2AX-positive matrix cells with mostly "nuclear foci" and weak "pan-nuclear" patterns at all time points (Fig. 7*C* and Fig. S10*D*). Furthermore, we showed that circadian changes in γH2AX expression are not accompanied by increased apoptosis, because cleaved caspase3-positive apoptotic cells were virtually absent in matrixes of both WT and $Cry1^{-/-};Cry2^{-/-}$ hair follicles at both CT50 and CT62 (Fig. S10*C*). To see whether circadian changes also exist in nucleotide excision repair pathway, we studied the expression of XPA, the only core nucleotide excision repair factor under the circadian control (17, 20, 21). Indeed, XPA expression was elevated in matrixes of WT hair follicles at CT62 versus CT50, whereas in $Cry1^{-/-};Cry2^{-/-}$, its expression levels were constantly high and arrhythmic (Fig. 7*B*). Together, these results support the role of intrinsic circadian clock in enforcing coordinated cell cycle checkpoint, likely allowing for matrix cells to undergo synchronous DNA damage repairs and for subsequent synchronous wave of mitotic divisions to occur (Fig. 7*D*).

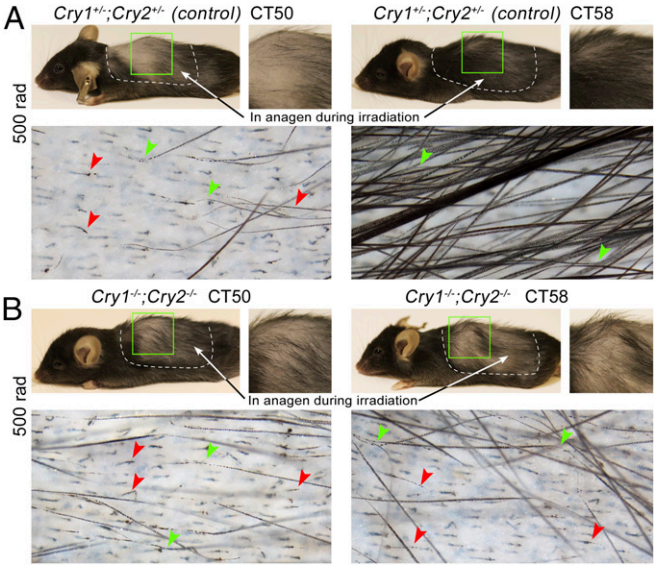

Fig. 6. Time-of-day–dependent radioprotective effect becomes lost in circadian mutants. (*A*) Significant differences in terms of hair loss are maintained in $Cry1^{+/-};Cry2^{+/-}$ heterozygous mice after 500 rad of irradiation. In the CT50 group, 96.9% of hairs broke, whereas in the CT58 group, almost 22.9% of hairs were still intact. (*B*) In $Cry1^{-/-};Cry2^{-/-}$ mutant mice irradiated with 500 rad, severe hair loss occurred both at CT50 and CT58 time points, with 90.8% and 92.3% broken hairs, respectively.

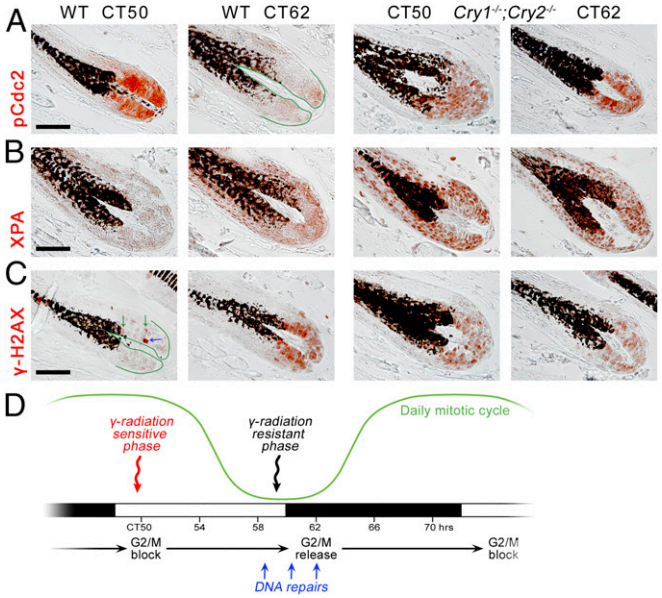

Fig. 7. Molecular profiling of cell cycle gating in the hair-follicle matrix. (*A*) In the matrix of WT hair follicles, pCdc2 (Tyr15) is expressed strongly at CT50 and yet greatly diminishes at CT62. These circadian differences disappear in *Cry1*$^{-/-}$;*Cry2*$^{-/-}$ mice, where pCdc2 expression becomes continuously strong. (*B*) Nuclear XPA is strongly elevated in the matrix of *Cry1*$^{-/-}$;*Cry2*$^{-/-}$ hair follicles compared with WT. (*C*) In the matrix of WT hair follicles, γH2AX has a large domain of strong nuclear expression at CT62 but not at CT50. These circadian differences disappear in *Cry1*$^{-/-}$;*Cry2*$^{-/-}$, where γH2AX becomes continuously strong. Also see Fig. S10. (*D*) Summary of circadian regulation of cell cycle, hair growth, DNA repairs, and genotoxic sensitivity in hair-follicle matrix. [Scale bars: 50 μm (*A*–*C*).]

Discussion

Here, we show that peripheral circadian clock is highly compartmentalized in regenerating hair follicles and that epithelial matrix and dermal papilla are key sites of circadian activity during the anagen phase of the hair-growth cycle. We demonstrate that cell-autonomous circadian oscillators in transient amplifying cells of the matrix generate daily mitotic rhythm, which makes hairs grow faster in the morning than in the evening. This daily mitotic rhythmicity also makes hair-growth sensitivity to ionizing radiation a time-of-day–dependent function. We show that growing hairs are remarkably more resistant to the same doses of γ-irradiation in the evening, during the mitotic depression than in the morning, during the mitotic peak.

Distinct Roles of Circadian Clock in Stem Cells and Transient Amplifying Cells During the Hair Cycle. These findings significantly extend our understanding of the circadian biology of the hair follicle. They complement previous works by Lin et al. (6) and Janich et al. (7) that uncovered the role of circadian clock in regulating quiescence and activation of hair follicle stem cells and hair germ progenitors. The original study by Lin et al. (6) demonstrated that the circadian clock promotes proliferation of hair germ cells during activation of telogen hair follicles and facilitates their progression through G_1/S cell cycle checkpoint. Interestingly, crosstalk between clock and cell cycle appears to be a common theme in the circadian biology of different epithelial cell types of the skin. Recent studies by Gaddameedhi et al. (17) and Geyfman et al. (8) showed that in epidermal keratinocytes, clock coordinates S-phase progression. Our own findings suggest that clock generates daily mitotic rhythmicity in hair matrix by synchronizing the Cdc2/Cyclin B-mediated G_2/M checkpoint. Indeed, the Cdc2-dependent G_2/M checkpoint is essential for normal mitotic progression and disruption of inhibitory Cdc2 phosphorylation results in mitotic desynchronization (22–24). Different checkpoint synchronization strategies between epidermis, hair germ, and hair-matrix cells are of interest and likely reflect general cell cycle synchronization strategies along lineages in other proliferating tissues and organs. The hair follicle matrix is one of the most proliferative cell populations in the body. It predominantly consists of committed transient amplifying cells and is spatially decoupled from hair follicle stem cells. By synchronizing mitotic entry, the circadian clock likely offers protection against endogenous genotoxic stress to the most sensitive M-phase subset of hair-matrix cells. This circadian effect becomes very obvious in our γ-irradiation experiments, where genotoxic response is tested at it upper limits. Interestingly, circadian G_2/M checkpoint synchronization strategy is also used during injury-induced regeneration of the liver (25). Similar to physiological hair regeneration, maximizing tissue size in the shortest possible period is one of the key goals of reparative organ regeneration. We speculate that circadian mitotic synchronization offers a well-balanced strategy for maintaining high rate of proliferation, while still offering genotoxic protection to the most sensitive subset of cells. Importantly, daily but not total mitotic output of hair matrix depends on circadian regulation. *Cry1*$^{-/-}$;*Cry2*$^{-/-}$ hair follicles do not have mitotic surplus and do not grow longer hairs than in WT. An additional, noncircadian mechanism, possibly driven by differentiation-inducing signaling such as WNT and/or BMP, likely regulates postmitotic exiting in hair precortex.

That proliferation in hair matrix is synchronized by cell-autonomous circadian rhythms, rather than by indirect signals generated by dermal papillae oscillator is significant. Robust oscillations in dermal papillae fibroblasts can, in principle, generate rhythmic paracrine signals for hair-matrix cells. Indeed, dermal papilla is the key regulator of matrix proliferation, and it produces several stimulating growth factors, including fibroblast growth factor 7 (Fgf7) and Fgf10. Loss of canonical WNT signaling in dermal papilla disrupts its stimulating effect on matrix and results in severe mitotic deficiency and shortened hairs (26). Because hair-matrix defects in induced *K14creER;Bmal1*$^{f/f}$ mice phenocopy those of *Cry1*$^{-/-}$;*Cry2*$^{-/-}$ mice, a model emerges where an intrinsic circadian clock in hair-matrix epithelial cells acts as the physiological modulator of their proliferation rhythm at the backdrop of a constant supply of dermal papilla-derived growth factors.

Diurnal Rhythm of Genotoxic Sensitivity in Rapidly Proliferating Cell Populations. One of the most striking effects of the circadian clock in our experiments was that on genotoxic sensitivity of growing hairs. We show that dramatic hair loss resistance in response to ionizing irradiation can be achieved in WT mice simply by timing γ-irradiation treatment to the time of the day with minimal mitotic activity in hair matrixes. These findings parallel daily changes in sensitivity of epidermis to external UV genotoxicity (8, 17, 27) and can have important implications for designing radiation therapy and possibly chemotherapy protocols. More immediately, radiation treatment can be administered during the mitotic depression phase to minimize hair loss side effect. In this respect, particularly interesting is the classic study that looked at the effect of skin hypothermia on the radiation sensitivity of growing hair follicles (28). This study exploited the fact that prolonged tissue cooling to 5–8 °C arrests mitotic progression and, in effect, produces artificial mitotic synchronization. Hair follicles were highly radiosensitive half an hour after hypothermia, during the induced mitotic peak, and their post-radiation survival significantly increased 5 h later, when M-phase matrix cells synchronously progressed into G_1.

Similar circadian synchronization strategy can be exploited to minimize side effects of radiation in other highly proliferative

tissues, most prominently gastrointestinal epithelium and bone marrow. This would, however, require gaining better understanding of the physiological mechanisms of cell cycle regulation by the circadian clock in these tissues. Alternatively, timing radiation delivery during the mitotic peak can be used to maximize its cytotoxic effect while minimizing the dose. This strategy can become especially useful in optimizing allogenic bone marrow replacement protocols for multiple myeloma or leukemia. Further proof-of-principle studies will be required in this direction. For such strategies to be viable, the circadian biology of cancer cells also has to be considered. Many types of cancer have an aberrant circadian clock (29), whereas mitotic progression in other types of cancer becomes asynchronous despite functional circadian oscillator (30, 31). The concept of cancer chronotherapy that considers timing radio- and chemotherapy to maximize its cytotoxicity on tumor cells is continuing to gain experimental support (32).

In conclusion, in this study, we used the model of regenerating hair follicle to learn about the role of circadian clock in highly proliferative cell populations. We show that by synchronizing DNA-damage repairs with cell cycle progression at the G_2/M checkpoint clock offers an additional layer of protection against disrupting effect of genotoxic stresses (33) and likely provides a complex hair follicle regenerative system with an advantage over long run. This long-term advantage is exemplified by the extremely rare occurrence of malignant hair follicle-derived tumors (34). Current findings extend our understanding of complex hair-cycle clockwork. It becomes clear that hair-cycle progression is regulated by several simultaneously acting mechanisms (35, 36). Circadian rhythms can modulate hair cycle both via peripheral (refs. 6 and 7 and this study) and central mechanisms. Unlike the peripheral mechanism, the central mechanism mediates seasonal changes and affects hair cycle in a more global way, likely via prolactin and other hormonal cues (37).

Methods

Animal Procedures. All animal experiments were carried out in accordance with the guidelines of the Institutional Animal Care and Use Committee of the Salk Institute and University of Southern California.

Experimental Mouse Models. *Per2*^{Luciferase} (*Per2*^{Luc}), *Cry1*$^{-/-}$;*Cry2*$^{-/-}$, and *K14creER;Bmal1*$^{f/f}$ transgenic mice were used in this study. *K14creER;Bmal1*$^{f/f}$ mice were generated by crossing *K14creER* mice (from Krzysztof Kobielak, University of Southern California, Los Angeles, CA) with *Bmal1*$^{f/f}$ [B6.129S4 (Cg)-*Arntl*^{tm1Weit}/J] mice (Jackson Laboratory; stock no. 007668). *Bmal1*$^{+}$ and *Bmal1*^{f} alleles were identified using PCR genotyping with the following primers: 5′-ACTGGAAGTAACTTTATCAAACTG-3′ (forward) and 5′-CTGACC-AAC TTGCTA ACA ATTA-3′ (reverse). Mice homozygous for *Bmal1*^{f} had a single band at 431 bp. Heterozygous mice had two bands: 431 and 327 bp (*Bmal1*$^{+}$) (Fig. 2*C*). The presence of Cre recombinase was identified using PCR method with the following primers: 5′-TTGCCCCTGTTTCACTATCCAG-3′ (forward) and 5′-ATGGATTTCCGTCTCTGGTG-3′ (reverse). The expected PCR product was 335 bp. To induce conditional deletion of *Bmal1*, *K14creER;Bmal1*$^{f/f}$ mice were treated with tamoxifen (Sigma-Aldrich; T5648) diluted in 100% ethanol (EtOH) at 25 mg/mL when dorsal hair follicles were in telogen phase. For the first 3 d of treatment, 200 μL was applied to the back of shaved mice. For the subsequent 8 d of treatment, 100 μL of the working solution was applied to the back of the mice. In the control group, *K14creER;Bmal1*$^{f/f}$ mice were treated with EtOH vehicle only with the same volumes as the experimental mice. Induction efficiency under *K14creER* was tested in *K14creER;R26R* mice. *K14creER;R26R* mice were treated with tamoxifen following an identical protocol, and induction efficiency was assessed based on lacZ staining. High levels of β-galactosidase expression were seen throughout dorsal skin epithelia (Fig. S7*E*).

Irradiation Experiments. Full-body irradiation using sublethal doses of γ-radiation, ranging from 400 to 700 rad, was administered to mice in which portion of dorsal hair follicles was in anagen phase. Seven-week-old mice entrained to 12-h light:12-h dark (LD) cycles were used in these experiments. Initially, approximately two-thirds of the dorsal hairs in these mice were depilated to induced synchronous anagen entry. Irradiation was performed 12 d later (at CT50 and CD58 experimental time points) when hair follicles in the depilated areas were in mature anagen phase, whereas undepilated hair follicles in the rest of the dorsal skin were in the second physiological telogen phase. The extent of radiation-induced hair loss was analyzed 7 d after irradiation; at which time point, plucking-induced anagen hair follicles reentered telogen phase.

Kinetic Real-Time Luminescence Measurements. Sixteen- to twenty-week-old *Per2*^{Luc} mice were euthanized and ∼5 × 5 mm patches of dorsal skin in anagen or telogen hair-cycle stages were excised. Several (10) skin patches were cultured together in Phenol Red-free DMEM [Gibco; supplemented with 10% FBS, 15 mM Hepes (pH 7.4), nonessential amino acids, sodium pyruvate, 1% penicillin/streptomycin/antimycotic, and 100 μM luciferin) in 3.5-cm dishes that were covered with sterile glass coverslips using vacuum grease. Luminescence levels were measured for several days in a Lumicycle luminometer (Actimetrics) as described previously (38). For luminescence measurement of single vibrissae follicles, mystacial pads were excised and single follicles were microdissected, which included removal of collagen capsule. The follicles were cultured in 3.5-cm dishes at 37 °C in previously described hair culture medium (39) based on Williams E medium supplemented with L-glutamine (2 mM), insulin (10 μg/mL), hydrocortisone (10ng/mL), 1% penicillin/streptomycin/antimycotic, and 100 μM luciferin. Shafts of the cultured follicles were immobilized in silicone on the bottom of the dish (40). Luminescence of the follicles was recorded in 30-min bins using a camera setup as described previously (38). Background correction and quantitative analysis of the resulting images were done using Metamorph Offline Version 7.5 (Molecular Devices). To better visualize recorded luminescence levels, gradient map filter using blue-to-red gradient was applied to snapshot images in the Adobe Photoshop software package, so that the darkest pixels of the image were converted to blue and the lightest pixels (corresponding to higher levels of luminescence) were converted to red.

Hair-Length Measurements. Club hair length was compared between adult (>100 d old) WT and *Cry1*$^{-/-}$;*Cry2*$^{-/-}$ mice. For the vibrissae, because of the significant natural length variability, comparison was done on club vibrissae only from the positionally identical follicles. Position of the vibrissae follicles was identified based on the established map of the mystacial pad (Fig. S8). Largest vibrissae from the two most caudal vertical rows (follicle positions E, F, G, H, and AI through AV) were compared. For the pelage, telogen club hairs were collected from the interscapular area of the dorsum. When selecting hairs for analysis, great care was taken to exclude hairs that had broken distal tips (typical for vibrissae) or did not have typical club morphology of the proximal end. Pelage hairs of guard and zigzag types were compared. Club hair length was measured as follow. Hairs, both vibrissae and pelage, were flattened between two glass slides, and digital pictures were taken. Because many hairs are naturally curved and/or bent, photographs of all club hairs were traced, and length of the resulting curve traces were measured in the Adobe Illustrator software package. Upon calibration of the traces, club hair length in millimeters was established. This method yields high precision and high resolution (±0.1 mm) of the measurements.

Skin Sample Collection. Sixteen- to twenty-week-old WT and *Cry1*$^{-/-}$;*Cry2*$^{-/-}$ mice were entrained to LD. *K14creER;Bmal1*$^{f/f}$ mice were similarly entrained upon completion of tamoxifen treatment. At the same time, the fur of all experimental mice was periodically clipped as it was growing, to reveal hair-cycle stages across entire dorsal skin. When appropriate hair-cycle waves developed, mice were released into constant darkness (DD). Fifty hours (CT50) after they were released into constant darkness dorsal skin containing hair-cycle wave(s) and mystacial pads with vibrissae were collected every 4 h for 24 h for WT mice and at CT50 and CT62 for *Cry1*$^{-/-}$;*Cry2*$^{-/-}$ and *K14creER;Bmal1*$^{f/f}$ mice.

Histology and Immunohistochemistry. Immunostaining was performed on paraffin sections. When necessary, antigen retrieval was performed by heating histologic sections in citric buffer. Considerable care was taken to ensure consistency of immunostaining protocol across all samples collected across all CTs. The primary antibodies used were rabbit anti-Per2 (1:200; Alpha Diagnostic), rabbit anti-Clock (1:400; Abcam), mouse anti-Npas2 (1:200; Abnova), mouse anti-Pcna (1:200; Abcam), rabbit anti-pH3 (Ser10) (1:100; Cell Signaling Technology), rabbit anti-cMyc (1:200; Santa Cruz Biotechnology), rabbit anti-phospho-CyclinD1 (Thr286) (1:50; Cell Signaling Technology), rabbit anti-pCdc2 (Tyr15) (1:50; Cell Signaling Technology), rabbit anti-pH2AX (Ser139) (1:100; Cell Signaling Technology), rabbit anti-XPA (1:200; Abcam), rabbit anti-cleaved caspase-3 (Asp175) (1:100; Cell Signaling Technology), rabbit anti-Lef1 (1:100; Cell Signaling Technology), rabbit anti-pSmad1/5/8 (1:50; Cell

Signaling Technology), mouse anti-AE15 (1:200; Santa Cruz Biotechnology), rabbit anti-keratin (Krt)14 (1:400; Berkeley Antibody), chicken anti-Krt15 (1:400; Covance), and mouse anti-8OHdG (1:200; Abcam). The 3-amino-9-ethylcarbazole (AEC) substrate kit for peroxidase (Vector Laboratories) was used for color development. Some stained samples were treated with H_2O_2 to bleach follicular melanin. In these cases, samples were photographed before and after bleaching and precise outlines of pigmented areas were reconstructed by digitally overlapping before and after images. Intensity of AEC substrate color was not affected by H_2O_2 (Fig. S7 *A–D*).

Pulse-chase labeling was performed using EdU nucleoside analog to thymidine (Invitrogen). A single dose of 50 μg/g EdU was administered i.p., followed by 36 h of chase. EdU detection was performed using the Click-iT EdU Alexa Fluor488 imaging kit using manufacturer's protocol (Invitrogen).

Histomorphometry. For comparative quantitative analysis of pH3-positive cells in the follicular matrix, digital pictures of all anagen hair follicles from pH3-stained 5-μm-think sections were taken at 400× magnification. For every hair follicle section, we counted the number of pH3-positive cells. For vibrissae follicles, we have normalized the number of pH3-positive cells per matrix per section relative to the diameter of the epithelial matrix at the Auber line level to compensate for the variability of the vibrissae size. A different morphometric technique was used for pelage follicles to compensate for more significant variability of the histologic section plane across the epithelial matrix. For pelage follicles, we counted the number of pixels occupied by the follicular matrix below the Auber line, as measured with the Histogram functionality of traced digital pictures in the Adobe Photoshop software package. Images were then calibrated, and traced areas of the follicular matrix were converted from pixels to square micron. In the end, the average numbers of pH3-positive cells per 10,000 μm^2 of the follicular matrix were established for every CT for both WT, *Cry1*$^{-/-}$*;Cry2*$^{-/-}$, and *K14creER;Bmal1*$^{f/f}$ pelage hair follicles.

ACKNOWLEDGMENTS. This work is supported by National Institute of Arthritis and Musculoskeletal and Skin Diseases Grants AR 42177 and 47364 (to C.-M.C.). S.P., A.C., and C.V. are supported by National Institutes of Health Grants DK091618 and P30 CA014195, American Diabetes Association Grant 7-12-MN-64, The Leona M. and Harry B. Helmsley Charitable Trust, Dana Foundation, and Glenn Foundation for medical research. M.V.P. is supported by the Edward Mallinckrodt Jr. Foundation Research Grant.

1. Reppert SM, Weaver DR (2002) Coordination of circadian timing in mammals. *Nature* 418(6901):935–941.
2. Panda S, Hogenesch JB, Kay SA (2002) Circadian rhythms from flies to human. *Nature* 417(6886):329–335.
3. Paus R, Müller-Röver S, Botchkarev VA (1999) Chronobiology of the hair follicle: Hunting the " hair cycle clock". *J Investig Dermatol Symp Proc* 4(3):338–345.
4. Paus R, Foitzik K (2004) In search of the "hair cycle clock": A guided tour. *Differentiation* 72(9-10):489–511.
5. Tanioka M, et al. (2009) Molecular clocks in mouse skin. *J Invest Dermatol* 129(5): 1225–1231.
6. Lin KK, et al. (2009) Circadian clock genes contribute to the regulation of hair follicle cycling. *PLoS Genet* 5(7):e1000573.
7. Janich P, et al. (2011) The circadian molecular clock creates epidermal stem cell heterogeneity. *Nature* 480(7376):209–214.
8. Geyfman M, et al. (2012) Brain and muscle Arnt-like protein-1 (BMAL1) controls circadian cell proliferation and susceptibility to UVB-induced DNA damage in the epidermis. *Proc Natl Acad Sci USA* 109(29):11758–11763.
9. Comaish S (1969) Autoradiographic studies of hair growth in various dermatoses: Investigation of a possible circadian rhythm in human hair growth. *Br J Dermatol* 81(4):283–288.
10. Potten CS, Jessup BA, Croxson MB (1971) Incorporation of tritiated thymidine into the skin and hair follicles. II. Daily fluctuations in 3 H-TdR and 3 H-UR levels. *Cell Tissue Kinet* 4(5):413–421.
11. Yoo SH, et al. (2004) PERIOD2:LUCIFERASE real-time reporting of circadian dynamics reveals persistent circadian oscillations in mouse peripheral tissues. *Proc Natl Acad Sci USA* 101(15):5339–5346.
12. Yano K, Brown LF, Detmar M (2001) Control of hair growth and follicle size by VEGF-mediated angiogenesis. *J Clin Invest* 107(4):409–417.
13. Sharov AA, et al. (2006) Bone morphogenetic protein signaling regulates the size of hair follicles and modulates the expression of cell cycle-associated genes. *Proc Natl Acad Sci USA* 103(48):18166–18171.
14. Terasima T, Tolmach LJ (1961) Changes in x-ray sensitivity of HeLa cells during the division cycle. *Nature* 190:1210–1211.
15. Sinclair WK, Morton RA (1965) X-ray and ultraviolet sensitivity of synchronized chinese hamster cells at various stages of the cell cycle. *Biophys J* 5:1–25.
16. Nakayama M, Kaida A, Deguchi S, Sakaguchi K, Miura M (2011) Radiosensitivity of early and late M-phase HeLa cells isolated by a combination of fluorescent ubiquitination-based cell cycle indicator (Fucci) and mitotic shake-off. *Radiat Res* 176(3):407–411.
17. Gaddameedhi S, Selby CP, Kaufmann WK, Smart RC, Sancar A (2011) Control of skin cancer by the circadian rhythm. *Proc Natl Acad Sci USA* 108(46):18790–18795.
18. Khapre RV, Samsa WE, Kondratov RV (2010) Circadian regulation of cell cycle: Molecular connections between aging and the circadian clock. *Ann Med* 42(6): 404–415.
19. Kondratov RV, Kondratova AA, Gorbacheva VY, Vykhovanets OV, Antoch MP (2006) Early aging and age-related pathologies in mice deficient in BMAL1, the core component of the circadian clock. *Genes Dev* 20(14):1868–1873.
20. Sancar A, et al. (2010) Circadian clock control of the cellular response to DNA damage. *FEBS Lett* 584(12):2618–2625.
21. Kang TH, Sancar A (2009) Circadian regulation of DNA excision repair: Implications for chrono-chemotherapy. *Cell Cycle* 8(11):1665–1667.
22. Park M, et al. (2000) Constitutive activation of cyclin B1-associated cdc2 kinase overrides p53-mediated G2-M arrest. *Cancer Res* 60(3):542–545.
23. Stumpff J, Duncan T, Homola E, Campbell SD, Su TT (2004) Drosophila Wee1 kinase regulates Cdk1 and mitotic entry during embryogenesis. *Curr Biol* 14(23):2143–2148.
24. Jin Z, Homola E, Tiong S, Campbell SD (2008) Drosophila myt1 is the major cdk1 inhibitory kinase for wing imaginal disc development. *Genetics* 180(4):2123–2133.
25. Matsuo T, et al. (2003) Control mechanism of the circadian clock for timing of cell division in vivo. *Science* 302(5643):255–259.
26. Enshell-Seijffers D, Lindon C, Kashiwagi M, Morgan BA (2010) Beta-catenin activity in the dermal papilla regulates morphogenesis and regeneration of hair. *Dev Cell* 18(4): 633–642.
27. Mitra S (2011) Does evening sun increase the risk of skin cancer? *Proc Natl Acad Sci USA* 108(47):18857–18858.
28. Dubravsky N, Hunter N, Withers HR (1976) The effect of precooling on the radiation sensitivity of the proliferating hair follicle. *Radiat Res* 65(3):481–489.
29. Lee JH, Sancar A (2011) Circadian clock disruption improves the efficacy of chemotherapy through p73-mediated apoptosis. *Proc Natl Acad Sci USA* 108(26): 10668–10672.
30. Yeom M, Pendergast JS, Ohmiya Y, Yamazaki S (2010) Circadian-independent cell mitosis in immortalized fibroblasts. *Proc Natl Acad Sci USA* 107(21):9665–9670.
31. Pendergast JS, Yeom M, Reyes BA, Ohmiya Y, Yamazaki S (2010) Disconnected circadian and cell cycles in a tumor-driven cell line. *Commun Integr Biol* 3(6):536–539.
32. Ramsey MR, Ellisen LW (2011) Circadian function in cancer: Regulating the DNA damage response. *Proc Natl Acad Sci USA* 108(26):10379–10380.
33. Gorbacheva VY, et al. (2005) Circadian sensitivity to the chemotherapeutic agent cyclophosphamide depends on the functional status of the CLOCK/BMAL1 transactivation complex. *Proc Natl Acad Sci USA* 102(9):3407–3412.
34. Alsaad KO, Obaidat NA, Ghazarian D (2007) Skin adnexal neoplasms—part 1: An approach to tumours of the pilosebaceous unit. *J Clin Pathol* 60(2):129–144.
35. Plikus MV, et al. (2011) Self-organizing and stochastic behaviors during the regeneration of hair stem cells. *Science* 332(6029):586–589.
36. Plikus MV (2012) New activators and inhibitors in the hair cycle clock: Targeting stem cells' state of competence. *J Invest Dermatol* 132(5):1321–1324.
37. Nixon AJ, et al. (2002) Regulation of prolactin receptor expression in ovine skin in relation to circulating prolactin and wool follicle growth status. *J Endocrinol* 172(3): 605–614.
38. Welsh DK, Yoo SH, Liu AC, Takahashi JS, Kay SA (2004) Bioluminescence imaging of individual fibroblasts reveals persistent, independently phased circadian rhythms of clock gene expression. *Curr Biol* 14(24):2289–2295.
39. Philpott MP, Green MR, Kealey T (1992) Rat hair follicle growth in vitro. *Br J Dermatol* 127(6):600–607.
40. Lee J, Wu W, Kopan R (2008) Murine vibrissae cultured in serum-free medium reinitiate anagen. *J Invest Dermatol* 128(2):482–485.